

The Influence Of Addition Of LiF And Complexing Agents Ethylene Diamine (en) And Acetyl Acetate (acac) On The Morphology And Topology Of The Deposited Ni Films From Deep Eutectic Solvents Type (III) Ethaline Using AFM Technique

K. El ttaib* and A. Benhmid

Department of Chemistry, Faculty of Science, University of Benghazi, Libya P.O. Box 1308
Corresponding Author: K. El ttaib

Abstract: The morphology and topology of nickel films in absence and presence of additives LiF, ethylene diamine (en) and acetyl acetate (acac) from ethylene glycol / choline chloride (ethaline), based ionic liquid on copper substrate, have been examined by AFM technique. The surface analysis was carried out by software nanoscope using surface roughness, section, power spectral densities (PSD), depth and width. The results showed that the average roughness (R_a), Root mean square roughness (R_q), the kurtosis (R_{ku}) and skew (R_{sk}) parameters showed that the distribution of spikes are perfectly random for Ni coating in absence of additives, bumpy in the presence of LiF, spiky in the presence of en and bumpy in the presence of acac. The power spectral densities raw data also show different lateral (x,y) values of spatial frequency, roughness skewness (R_{sk}) values for Ni deposits in absence and presence of ethylene diamine and acetyl acetate, moreover it has been found that the addition of LiF can act as brightener and shows significant influence on the formation of Ni deposits.

Key words: ethaline, Ni deposits, ionic liquids, LiF, surface roughness, RMS and morphology

Date of Submission: 17-01-2020

Date of Acceptance: 04-02-2020

I. Introduction

Physical chemists and physicists necessitate precise-scale details of surfaces and frequently details of molecular roughness. [1-2] Surface roughness is generally characterized by the standard deviation of surface heights. These features and information are usually supplied utilizing methods such as low-energy electron diffraction, molecular-beam methods, field-emission, field-ion microscopy, scanning tunneling microscopy, and atomic force microscopy which is used in this study. Surface roughness is most frequently associated with the dissimilarities in the height of the surface relative to a reference plane. It is determined by either along a single line profile or along a set of parallel line profiles (surface maps). These are R_a , the average roughness) and R_q or root mean square. Height designators are skewness (R_{sk}) and kurtosis (R_K). The other parameters that can be utilized are R_p (maximum peak height, maximum peak-to-mean height or simply P-M distance), R_v (maximum valley depth or mean-to-lowest valley height), R_z (average peak-to-valley height), and R_{pm} (average peak-to-mean height) which depicted in Figure 1.

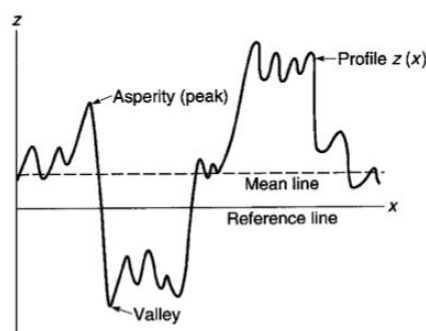


Figure 1 shows that the measurements of R_a , R_q and the standard deviation σ is the square root of the arithmetic mean of the square of the vertical deviation ($z(x)$) from the mean line [3-4].

It can be expressed mathematically

$$R_a = \frac{1}{L} \int_0^L |z - m| dx \quad (1)$$

$$= \frac{1}{L} \int_0^L z dx$$

Where L is the profile length

$$M_0 = \sigma^2 = \frac{1}{L} \int_0^L (z - m)^2 dx \quad (2)$$

$$M_2 = (\sigma')^2 = \frac{1}{L} \int_0^L \left(\frac{dz}{dx}\right)^2 dx \quad (3)$$

$$M_4 = (\sigma'')^2 = \frac{1}{L} \int_0^L \left(\frac{d^2z}{dx^2}\right)^2 dx \quad (4)$$

where σ' and σ'' are the standard deviations of the first and second derivatives of the functions. For a surface/profile height, these are the surface/profile slope and curvature, respectively.

$$\sigma^2 = R_q^2 - m^2$$

The zeroth moment ($n = 0$) is equal to 1. The first moment is equal to m , mean value of the function $z(x)$, whereas the first central moment is equal to zero [5].

According to [6], a random and isotropic surface with a Gaussian height distribution can be adequately characterized by the three zeroth (M_0), second (M_2) and fourth moments (M_4) of the power spectral density function [7].

For completeness, we note that

$$m = \frac{1}{L} \int_0^L z dx = 0$$

then $R_q = \sigma$

for Gaussian surfaces,

$$\sigma \approx \sqrt{\frac{\pi}{2}} R_a \approx 1.25 R_a \quad (5)$$

It is possible, for surfaces of widely differing profiles with different frequencies or wavelength and different shapes, to give the same R_a or σ (R_q) values as shown in the figure 2.

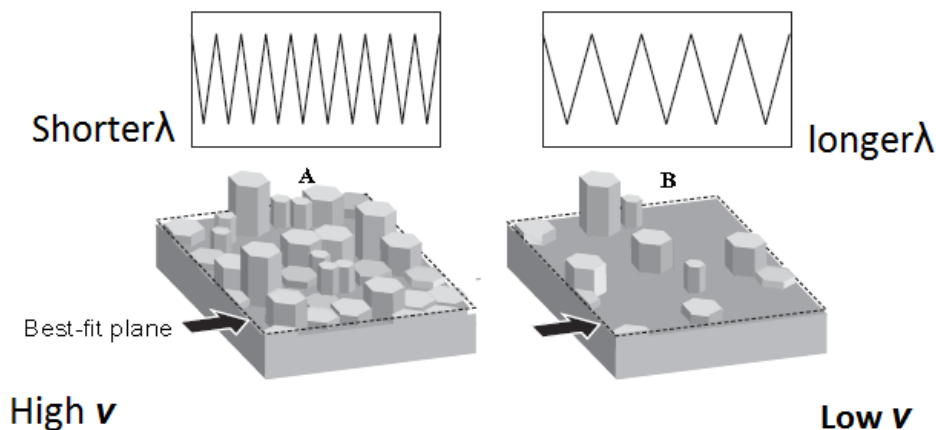


Figure 2 shows schematic two surfaces have equal surface roughness (vertical) R_a and R_q but different spatial frequency (lateral (x, y)).

To distinguish between surfaces have same values of R_a or σ (R_q) you can count on power spectral densities or other statistical parameters. Authors reported that the variances of surface height and its derivatives and other roughness parameters depend strongly on the resolution of the roughness measuring instrument or any other form of filter; hence they are not unique for a surface [8-10].

Power Spectral Density (PSD)

The Power Spectral Density (PSD) in NanoScope Software 6.13 User Guide is one of the surface texture descriptors which is a good tool for analyzing lateral surface roughness (x, y). This function comes with a representation of the amplitude of a surface's roughness as a function of the spatial frequency of the roughness. Spatial frequency is the inverse of the wavelength of the roughness features. The PSD function reveals periodic surface features that might otherwise appear random and provides a graphic representation of how such features are distributed. On turned surfaces, this is helpful in determining speed and feed data, sources of noise, etc. On ground surfaces, this may unveil some intrinsic features of the material itself such as grain or fibrousness. At higher magnifications, PSD is also useful for determining atomic periodicity or lattice [1].

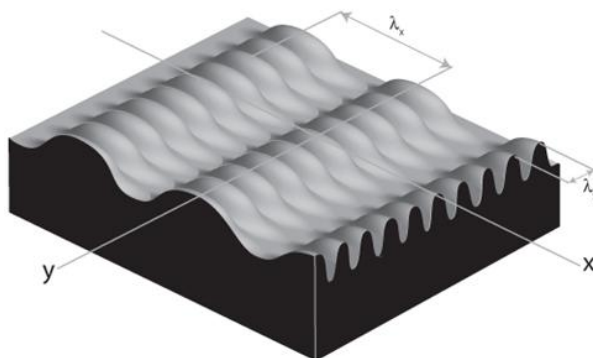


Figure 3a waveform spectrum (2D spectrum).

A 2-dimensional power spectral density plot of this surface would involve two dominant spikes (one for each superior wavelength), plus some number of extra wavelengths intrinsic within the image. (These extra wavelengths may reveal due to fine surface features and/or side bands of the dominant wave forms). Because of the sine wave nature of the composite wave form, a relatively small set of spectral frequencies suits to delineate the entire surface. By contrast, an image comprised of angular (saw-toothed or square) waveform contains more spatial frequency components.

PSD and Flatness

Surface roughness is generally characterized by the standard deviation of surface heights [5]. Compare two surfaces with sinusoidal waveforms with the same peak height, but different wavelengths. Researchers [6-11] have shown that they will have the same R_a and σ , but with different spatial display of surface altitude. Power Spectral Density (PSD) is one of the tools that offer a means of introducing the feature of all wavelengths. Gaussian surfaces might be thought as containing a certain number of asperities (hills) and an equal number of valleys. These properties may be examined and shown by their appropriate distribution curves, which can be described by the same type of features as were utilized previously for the surface peak heights and valleys often follow the Gaussian curve [12-14]. The distribution curves can also be obtained for the absolute values of slope and for the curvature of the peaks (or summits) and valleys. Distributions of peak (or summit) curvature follow a log normal distribution. The mean of the peak curvature increases with the peak height for a given surface [15-17]. PSD is used increasingly as a metrology tool for evaluating extremely flat surfaces, such as polished or epitaxial silicon. Generally, the desired surface is expected to adhere to certain PSD thresholds, signifying it meets a specified flatness criterion. The main advantage gained over traditional R_a specifications is that PSD flatness is qualified through the full spectral range of interest. For example, one may specify spectral thresholds at frequencies measured on the atomic scale, thus confirming surfaces contain largely uniform lattices. Setting the precise thresholds for various materials remains a matter of discussion.

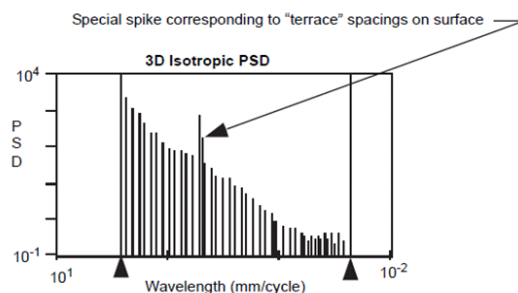


Figure 3b shows power spectral densities (PSD) chart terraced surface.

This narrow PSD plot is characteristic of flat, isotropic surfaces. Longer wavelengths are present up to the scan width, and are accompanied by evenly decreasing powers of shorter wavelengths down to 2 pixels. On the plot shown above a spike stands out, corresponding to the wavelength spacing of the terraced features. Depending upon the qualitative standards of the person evaluating such a plot, this spike may exceed a threshold standard of flatness.

Ionic liquids

The electrodeposition of numerous metals and alloys has been demonstrated using a variety of ionic liquids with both discrete and complex anions. Numerous reviews have been published on metal deposition using ionic liquids [18–22] and a recent book [23] provides an authoritative summary of the area. The advantages of these novel solvents include: electroplating electronegative metals, e.g. Al, Ta, Nb, Mo and W; direct electroplating of metal on water sensitive substrate materials such as Al and Mg can be achieved, removal of hydrogen embrittlement from the substrate; alloy deposition is easier to achieve; the possibility exists to develop novel immersion plating baths; potential energy savings compared with aqueous solutions; replacement of many hazardous and toxic materials currently used in water, e.g. Cr(VI), cyanide; and access to novel deposit morphologies. While the majority of important metals have been studied in these solvents, one obvious omission is the deposition of nickel. Gou and Sun [24] have recently studied the electrodeposition of nickel and nickel–zinc alloys from the zinc chloride–1-ethyl-3-methylimidazolium chloride. They found that although NiCl₂ dissolved in the pure chloride rich 1-ethyl-3-methylimidazolium chloride ionic melt, metallic nickel could not be obtained by electrochemical reduction of this solution. The addition of zinc chloride to this solution enabled the electrodeposition of dense, compact and adherent nickel coatings. It has recently been shown that ionic liquids can be formed from eutectic mixtures of a quaternary ammonium salt such as choline chloride (ChCl) with a hydrogen bond donor species such as a glycol, amide [25] or carboxylic acid [26]. These liquids have been used for the deposition of a range of metal coatings including Zn, Cr and Sn [27], Cu and Ag [28–29] and for metal dissolution processes such as electropolishing [30–31]. Here, the electrolytic deposition and morphologies of metallic Ni coatings from ionic liquids (IL) based on a ChCl ethylene glycol (EG) (1 : 2) respectively (Ethaline) eutectic mix were investigated. Changes in morphology and topology have been investigated by the addition of brighteners and used in the deposition process. It has been reported that the addition of alkali metal fluorides such as LiF has a significant effect upon the electrodeposition of metals in high temperature molten salts [32–35]. Furthermore the addition of LiF has been found to improve the mechanical properties of deposited films. Endres [36] and co-workers noticed that the morphology changed with the addition of LiF.

Materials and experimental

Choline chloride [HOC₂H₄N(CH₃)₃Cl] (ChCl) (Aldrich 99%) was recrystallised from absolute ethanol, filtered and dried under the vacuum. Ethylene glycol (Aldrich +99%), nickel chloride dihydrate, ethylenediamine (en) and acetylacetonate (acac) (all Aldrich) were all used as received. Ethaline is prepared by mixing one mole equivalent of Choline chloride with two mole equivalents ethylene glycol and stirring the mixtures together at 100°C until a homogeneous, colourless liquid is formed.

Atomic Force Microscopy (AFM) Surface Nano-characterization

The surface analysis in this investigation was carried out using a Digital Instrument Nanoscope IV Dimension 300 (Veeco) atomic force microscope with a 100 μm scanning head and run using both contact tapping (resonant) modes. Images were acquired in air. AFM is a very-high-resolution type of scanning probe microscopy (SPM), with demonstrated resolution on the order of fractions of a nanometer, more than 1000 times better than the optical diffraction limit. Studying the topology and morphology of variety of surfaces by AFM. AFM can provide very valuable and important information about mechanical mass production and [32],

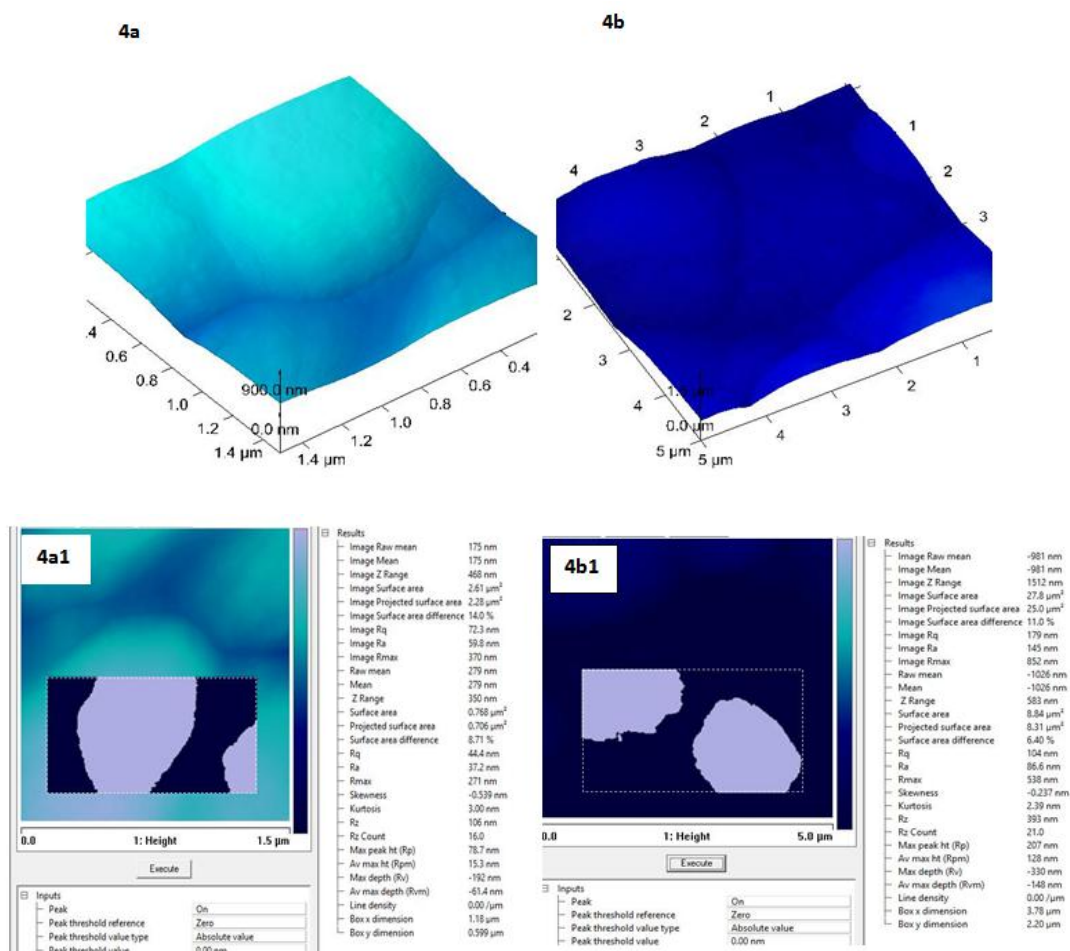
tribological properties [37, 38], where tribology field of active research that deals with for example friction and wear and thin film surfaces[39-40]. This tool can show the detail of surface texture better than other microscopic methods. Using appropriate software it is possible to assess features such as roughness, porosity, average size, and particle size distribution, which have great effect on the optical, mechanical, surface, magnetic and electrical properties of thin films. The goal of this work to examine the surface topology and morphology of the nickel deposits on copper substrate from deep eutectic solvent reline and compared with deposits with added leveling agents ethylene diamine and acetylacetonate (acac). The properties of deposits films and their nature have been investigated by parameters such as the average roughness, maximum peak to valley height, root mean square roughness, ten-point mean height roughness, power spectral density (PSD), surface skewness and surface kurtosis. However the surface analysis was carried out using a nanoscope IV Dimension 300 (Veeco) atomic force microscope with a 100 μm scanning head and using both contact and tapping (resonant) modes. Images were acquired in air.

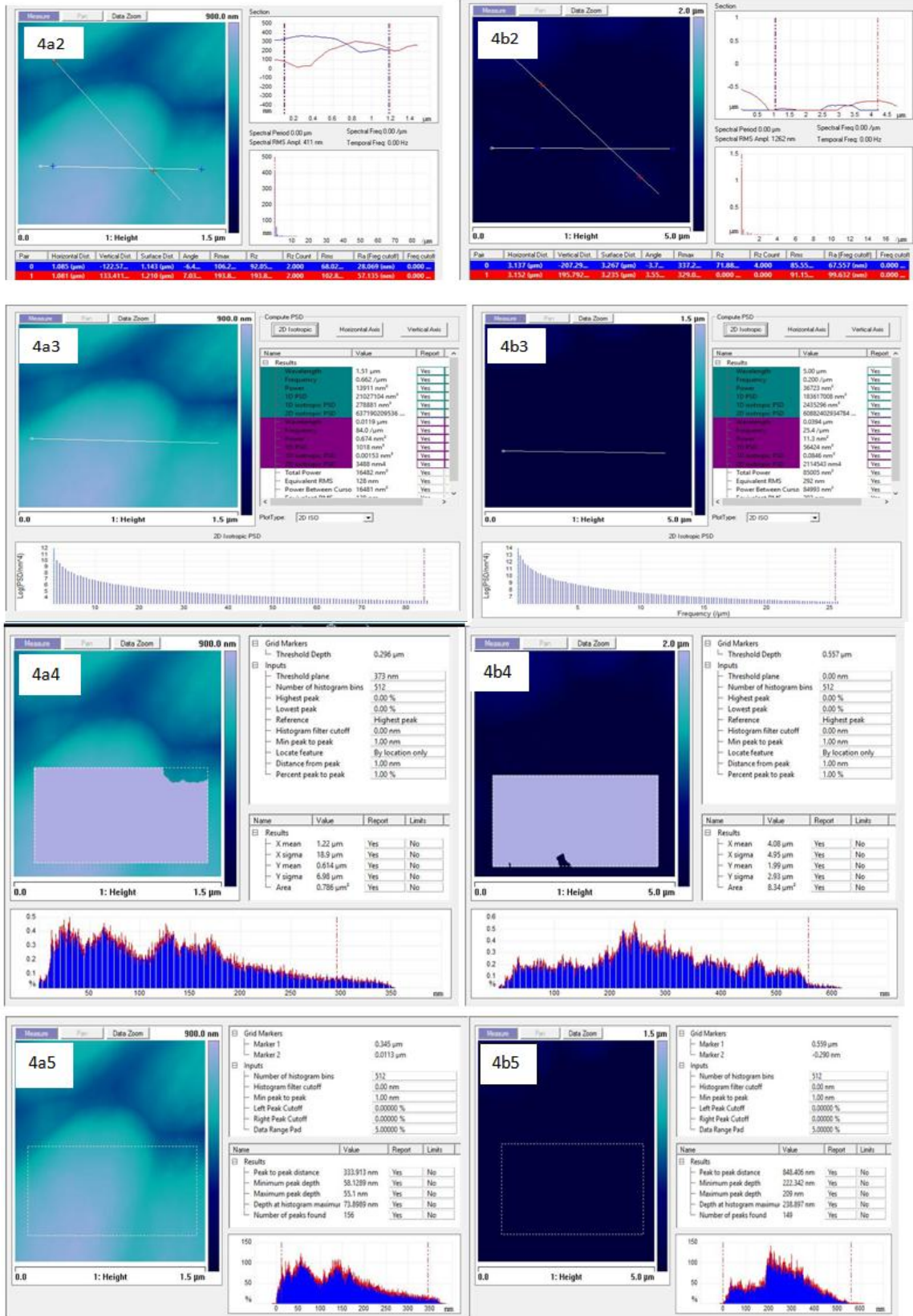
II. Result And Discussion

The magnitude variables of a sample are reported by variables which provide information about statistical average values, appearance of the histogram heights and other acute properties. The average roughness (R_a) is the mean height calculated over the entire measured length/area. R_a is typically used to feature the roughness of machined surfaces. It is applicable for diagnose general variations in overall profile height characteristics and for tracing a regular manufacturing process. Maximum peak to valley height roughness (R_z) is the vertical distance between the highest and lowest points in the evaluated length/area and describes the overall roughness of the surface. Root mean square (RMS) roughness (R_q) is the square root of the distribution of surface height and is considered to be more sensitive than the average roughness for large irregularity, from the mean line/plane and is also utilized in calculating the skew and kurtosis variables. RMS roughness (R_q) describes the finish of optical surfaces. It represents the standard deviation of the profile heights and is employed in calculations of skew and kurtosis. Ten-points mean height roughness (R_z) is the difference in height between the average of five highest peaks and five lowest valleys in the evaluation profile/surface and is more sensitive to occasional high peaks or deep valleys than R_z . Roughness skewness (R_{sk}) is used to measure the uniformity of the dissimilarity of a profile/surface about the mean line/plane and is more sensitive to occasional deep valleys or high peaks. R_{sk} determines load carrying capacity, porosity, and characteristics of atypical machining processes. Usually, R_{sk} is used to differentiate between two profiles of the same R_a or R_q values but of different shapes. Kurtosis is a measure of the distribution of spikes above and below the mean line. It is often specified for the control of stress fracture. Roughness kurtosis (R_{ku}) is used to measure the distribution of the spikes above and below the mean line/plane. For (spiky surfaces, $R_{ku} > 3$); (for bumpy surfaces, $R_{ku} < 3$); (perfectly random surfaces have kurtosis is equal to 3)[41]. With reference to Normal distribution, is presumed that, the correlation $R_q \approx 1.25 R_a$. Ward [42] observed that peak (asperity) height distribution of most engineering surfaces (tribology) may be estimated by a normal distribution with $R_q \approx 1.31 R_a$.

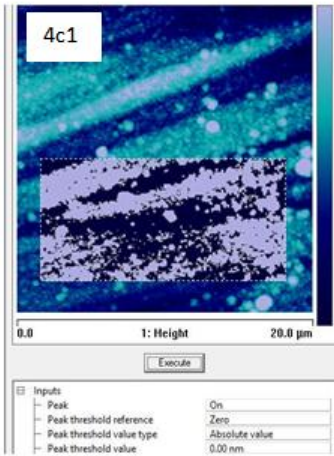
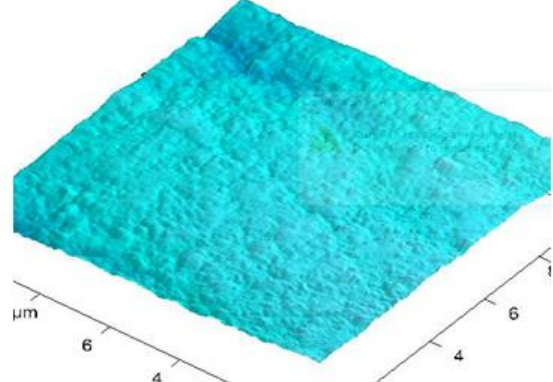
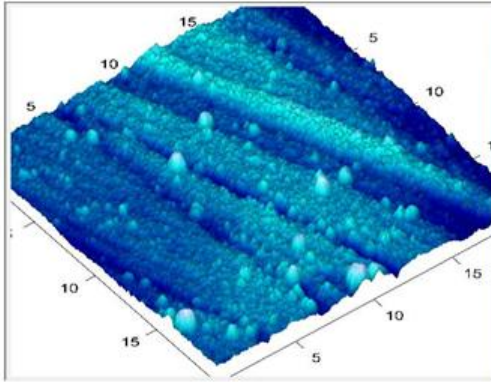
Figure 4 represents **a, b** with 1% LiF, **c** with en and **d** with acac showing AFM images for Ni coatings in presence and absence of additives, 4a1, 4b1, 4c1 and 4d1 depict roughness data for Ni coatings in presence and absence of additives, 4a2, 4b2, 4c2 and 4d2 explain section graphs and data for Ni deposits in presence and absence of additives, 4a3, 4b3, 4c3 and 4d3 represent power spectral density (PSD) information for Ni deposits in presence and absence of additives, 4a4, 4b4, 4c4, 4d4, 4a5, 4b5, 4c5, 4d5 represent the width and depth data for Ni deposits in presence and absence of additives respectively. The data obtained in Table 1 from AFM images are significantly valuable and important. It shows that the roughness value of the Ni coating was obtained to be 37.2 nm when the deposition was achieved in a bath without additives; however, the roughness of the Ni deposits increased to 86.6 nm and 51.7 nm when the coating was achieved from the same liquid medium in the presence of LiF and acac respectively, surprisingly the surface roughness of nickel deposits decreased to 28 nm in case of ethylene diamine is added. This was consistent with the results reported by Alesary[43], the addition of NaBr changes the surface morphology and roughness. Alesary[43] showed that the presence of additives creates a barrier between the nickel atoms and the active site of the substrate; this will lead to the change on the nucleation and the mechanism of growth. Moreover, the results of surface roughness obtained from Table 1 are compared to the results of surface roughness provided from Ni coating performed from reline[44] bath and it was noticed that the surface roughness of Ni deposits from ethaline and reline with added acac increases while the surface roughness decreases in the presence of en in case of ethaline electrolyte and increases in reline electrolyte. It is interesting to observe that the R_q / R_a ratio of Ni deposits with added acac from both electrolytes ethaline possesses the 1.24 value which is in the calculated range (1.25-1.31)[36-37]. Table 1 summarizes the values of Roughness kurtosis (R_{ku}) and roughness skewness (R_{sk}) nickel deposits from Ethaline in the absence and presence of additives and as it predicted the difference in the surface textures lead to values of Roughness kurtosis (R_{ku}) and roughness skewness (R_{sk}).

Figure 4 Shows AFM images and data for Ni films performed by ethaline bath in absence and presence of additives.



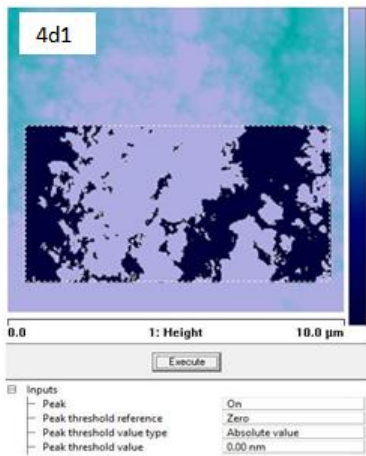


4c Ni electroplated in presence of en 4d Ni electroplated in presence of acac



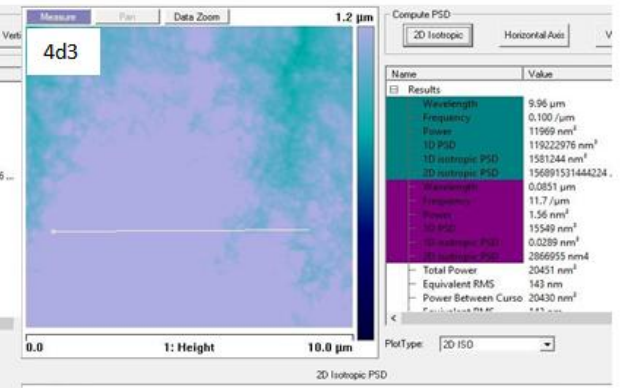
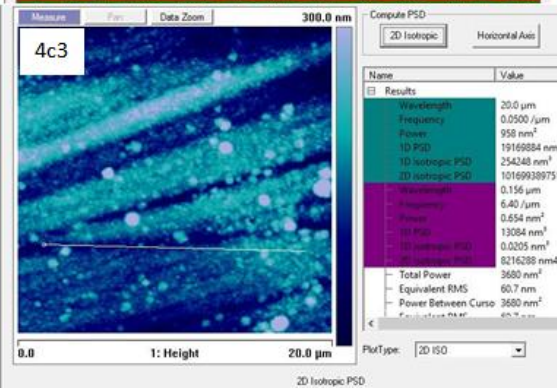
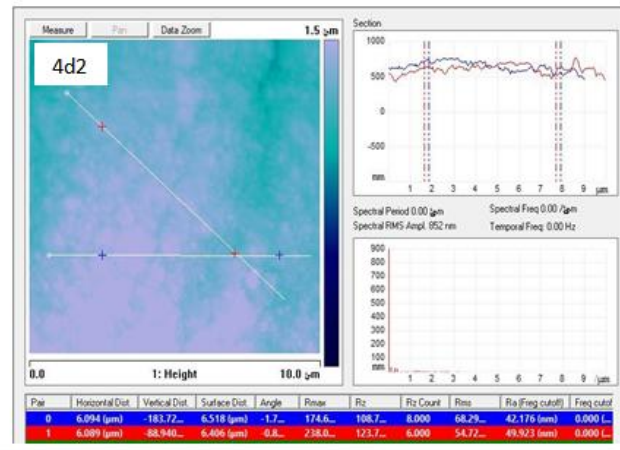
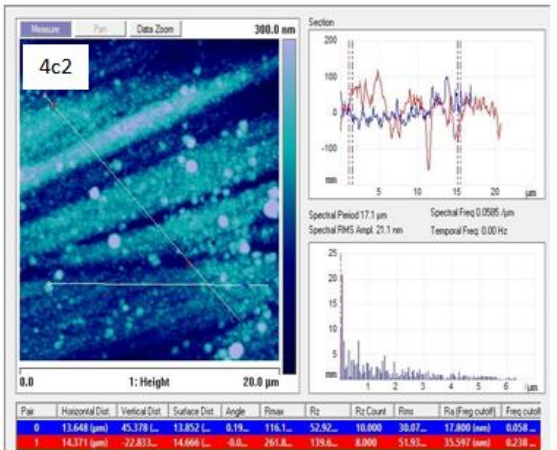
Results

- Image Raw mean: -222 nm
- Image Mean: 0.0225 nm
- Image Z Range: 583 nm
- Image Surface area: 418 μm²
- Image Projected surface area: 400 μm²
- Image Surface area difference: 4.51 %
- Image Rq: 57.9 nm
- Image Ra: 45.0 nm
- Image Rmax: 578 nm
- Raw mean: 67.5 nm
- Mean: 6.86 nm
- Z Range: 455 nm
- Surface area: 137 μm²
- Projected surface area: 132 μm²
- Surface area difference: 4.30 %
- Rq: 39.6 nm
- Ra: 28.0 nm
- Rmax: 462 nm
- Skewness: 0.295 nm
- Kurtosis: 7.21 nm
- Rz: 59.4 nm
- Rz Count: 842
- Max peak ht (Rp): 248 nm
- Av max ht (Rpm): 29.1 nm
- Max depth (Rv): -214 nm
- Av max depth (Rvm): -18.2 nm
- Line density: 0.00 /μm
- Box x dimension: 16.6 μm
- Box y dimension: 7.92 μm



Results

- Image Raw mean: 578 nm
- Image Mean: 578 nm
- Image Z Range: 753 nm
- Image Surface area: 112 μm²
- Image Projected surface area: 99.2 μm²
- Image Surface area difference: 13.1 %
- Image Rq: 83.4 nm
- Image Ra: 67.5 nm
- Image Rmax: 605 nm
- Raw mean: 635 nm
- Mean: 635 nm
- Z Range: 612 nm
- Surface area: 52.9 μm²
- Projected surface area: 46.4 μm²
- Surface area difference: 14.1 %
- Rq: 69.8 nm
- Ra: 56.3 nm
- Rmax: 585 nm
- Skewness: -0.380 nm
- Kurtosis: 2.86 nm
- Rz: 100 nm
- Rz Count: 994
- Max peak ht (Rp): 302 nm
- Av max ht (Rpm): 52.7 nm
- Max depth (Rv): -283 nm
- Av max depth (Rvm): -43.5 nm
- Line density: 0.00 /μm
- Box x dimension: 9.06 μm
- Box y dimension: 5.12 μm



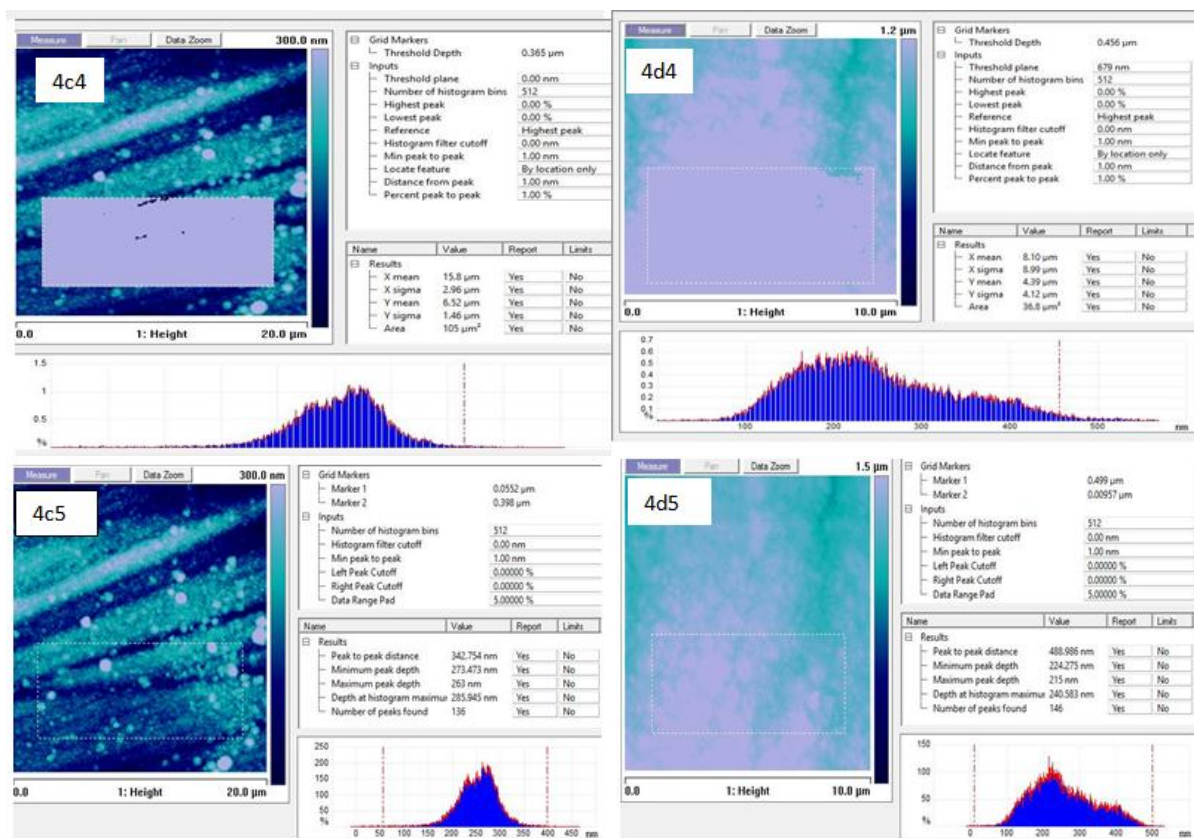


Table. 1 Roughness parameters of Nickel deposits with absence and presence of additives

Ni deposits from ethaline	R_a nm	R_q nm	R_z nm	R_q / R_a	R_{sk} nm	R_{ku} nm	Distribution Of spikes
Without addition	37.2	44.4	106	1.19	-0.539	3.00	Perfectly random
1% LiF	86.6	104	393	1.20	-0.237	2.39	bumpy
en	28	39.6	59.4	1.41	0.295	7.21	Spiky
acac	51.7	63.9	99.3	1.24	-0.202	2.75	bumpy

The distribution of spikes in absence of additives is perfectly random perfectly random ($R_{ku} = 3$)[36], and the negative value of R_{sk} tells that the surface has more valleys the peaks this is also the case of nickel coatings performed in the of LiF and acac but the nickel deposits obtained with added ethylene diamine (en) has positive value of roughness skewness (R_{sk}) which means the surface roughness has peaks than values, and the distribution of spikes is spiky ($R_{ku} = 3$)[36].

III. Conclusion

In this study, it is shown that the presence of additives resulted in changes in the morphology and topology, which can be clearly seen from the AFM images. However, the surface roughness values were found to be varied depending on the type of complexing agents, the power spectral densities raw data also show different lateral (x, y) values of spatial frequency, roughness skewness (R_{sk}) values for Ni deposits in absence and presence of ethylene diamine and acetyl acetate, which indicate that the surface textures had more valleys than peaks while the Ni films obtained performed in the presence of ethylene diamine had more peaks than valleys. The distribution of spikes are also different depending on the values of roughness kurtosis (R_{ku}) where Ni deposit without additives the distribution of spikes is perfectly random, bumpy surface for both Ni film coatings in the presence of LiF, acac and spiky peak distribution for Ni deposits with added ethylene diamine.

Reference

- [1]. Anonymous Instruments for the Measurement of Surface Roughness by Profile Methods, (1975), ISO3274, International Standardization Organization.
- [2]. Anonymous, Surface Texture (Surface Roughness, Waviness and Lay), (1985) ANSI/ASME B46.1, ASME, New York.
- [3]. Anonymous, Nanoscope III Scanning Tunneling Microscope, Instruction Manual, Digital Instruments, (1992a) Santa Barbara, CA.
- [4]. Anonymous, Nanoscope III Scanning Tunneling Microscope, Instruction Manual, Digital Instruments, (1992b) Santa Barbara, CA.
- [5]. B.Bhushan The Ohio State University © 2001 by CRC Press LLC.
- [6]. P. R. Nayak Random process model of rough surfaces, ASME J. Lub. Tech., (1971) 93, 398-407.
- [7]. P. R. Nayak Some aspects of surface roughness measurement, Wear (1973) 26, 165-174.
- [8]. C. D. McGillem, and G. R. Cooper Continuous and Discrete Signal and System Analysis, (1984) Holt, Rinehart & Winston, New York.
- [9]. C.Y. Poon, and B.Bhushan Comparison of surface roughness measurements by stylus profiler, AFM and non-contact optical profiler, Wear (1995a) 190, 76-88.
- [10]. C.Y. Poon, B.Bhushan Comparison of surface roughness analysis of glass-ceramic substrates, and finished magnetic disks, and Ni-P coated Al-Mg and glass substrates, Wear (1995b) 190, 89-109.
- [11]. J.S. Bendat, A. G. Piersol Engineering Applications of Correlation and Spectral Analysis, 2nd edition (1986) Wiley, New York.
- [12]. J. A. Greenwood A unified theory of surface roughness, Proc. R. Soc. London A (1984) 393, 133-157.
- [13]. J.C. Wyant Use of an ac heterodyne lateral shear interferometer with real time wavefront correction systems, Appl. Opt. (1975) 14, 2622-2626.
- [14]. J.C. Wyant, Computerized interferometric measurement of surface microstructure, Proc. Soc. Photo-Opt. Instrum. (1995) Eng., 2576, 122-130.
- [15]. J.C. Wyant, C. L. Koliopoulos Phase measurement system for adaptive optics Agard Conference proceedings, (1981) No. 300, 48.1-48.12.
- [16]. J.C. Wyant, C. L. Koliopoulos, B.Bhushan, O. E. George, surface characterization of magnetic media, ASLE Trans. (1984) 27, 101-113.
- [17]. J.C. Wyant, C.L. Koliopoulos, B.Bhushan, D. Basila, Development of a three-dimensional noncontact digital optical profiler ASME J. Trib. (1986) 108, 1-8.
- [18]. Endres F., Chem. Phys. Chem. (2002) 3, 144.
- [19]. Abbott A. P. and K. J. McKenzie: Phys. Chem. Chem. Phys. (2006) 8, 4265.
- [20]. H. Ohno (ed.): 'Electrochemical aspects of ionic liquids'; (2005) New York, John Wiley and Sons.
- [21]. F. Endres: Z. Phys. Chem. Chem. Phys. (2004) 218, 255.
- [22]. F. Endres and S. Zein El Abedin: Phys. Chem. Chem. Phys. (2006) 8, 2101.
- [23]. F. Endres, A. P. Abbott and D. R. MacFarlane: 'Electrodeposition of metals using ionic liquids'; (2008) Weinheim, Wiley-VCH.
- [24]. S.-P. Gou and I.-W. Sun: Electrochim. Acta, (2008) 53, 2538-2544.
- [25]. A. P. Abbott, G. Capper, D. L. Davies, R. Rasheed and V. Tambyrajah: Chem. Commun. (2003) 1, 70.
- [26]. A. P. Abbott, D. Boothby, G. Capper, D. L. Davies and R. Rasheed J. Am. Chem. Soc., (2004) 126, 9142.
- [27]. A. P. Abbott, S. Nandhra, S. Postlethwaite, K. S. Ryder and E. L. Smith: Phys. Chem. Chem. Phys. (2007) 9, 3735-3743.
- [28]. A. P. Abbott, J. Griffith, S. Nandhra, C. O'Connor, S. Postlethwaite, K. S. Ryder and E. Smith: Surf. Coat. Technol. (2008) 202, 2033-2039.
- [29]. A. P. Abbott, G. Capper, B. Swain and D. Wheeler: Trans. IMF, (2005) 82, 51-54.
- [30]. A. P. Abbott, J. Griffith, S. Nandhra, C. O'Connor, S. Postlethwaite, K. S. Ryder and E. Smith: Surf. Coat. Technol., (2008) 202, 2033-2039.
- [31]. A. P. Abbott, G. Capper, K. J. McKenzie and K. S. Ryder: Electrochim. Acta, (2006) 51, 4420-4425.
- [32]. A. J. B. Dutra, J. C. Vazques and A. Spinola, Min. Eng. (1993) 6, 663.
- [33]. P. Chamelot, P. Taxil and B. Lafage, Electrochim. Acta (1994) 39, 2571.
- [34]. P. Chamelot, P. Palau, L. Massot, A. Savall, P. Taxil, Electrochim. Acta, (2002) 47, 3423.
- [35]. F. Lantelme, A. Barhoun, G. Le, J. P. Besse J. Electrochem. Soc. (1992) 139, 1255.
- [36]. S. Zein El Abedin, H. K. Farag, E. M. Moustafa, F. Endres, Phys. Chem. Chem. Phys. (2005) 7, 2333.
- [37]. N. Jalili, K. Laxminarayana, Mechatronics, (2004) 14, 907.
- [38]. D. Marchetto, A. Rota, L. Calabri, G. C. Gazzadi, C. Menozzi, S. Valeri, Wear (2008) 265, 577.
- [39]. D. D. Nesheva, E. Vateva, Z. Levi, D. Arsova, J. Phys. Chem. Solids (2007) 68, 675.
- [40]. K.R. Nagabhushana, B.N. Lakshminarasappa, F. Singh, Nucl. Instr. and Meth. in Phys. Res. B, (2008) 266, 1040.
- [41]. B. Rajish Kumara, T. SUBBA RAO Digest Journal of Nanomaterials and Biostructures, October-December (2012) 4, 1881-1889.
- [42]. H.C. Ward, Rough Surfaces, T.R. Thomas Ed., Longman, London (1982).
- [43]. H.F. Alesary, A.F. Khudhair, S. Y. Rfaish, H. K. Ismail, Int. J. Electrochem. Sci. (2019) 14, 7116.
- [44]. K. Eltaib, A. Benhmidi IOSR Journal of applied chemistry (IOSR-JAC) (2019) 12, 15-22.